

# Emergence of Separable Manifolds in Deep Language Representations

Jonathan Mamou <sup>\*1</sup> Hang Le <sup>\*2</sup> Miguel A Del Rio <sup>2</sup> Cory Stephenson <sup>1</sup>  
 Hanlin Tang <sup>1</sup> Yoon Kim <sup>3</sup> SueYeon Chung <sup>2,4</sup>

## Abstract

Deep neural networks (DNNs) have shown much empirical success in solving perceptual tasks across various cognitive modalities. While they are only loosely inspired by the biological brain, recent studies report considerable similarities between representations extracted from task-optimized DNNs and neural populations in the brain. DNNs have subsequently become a popular model class to infer computational principles underlying complex cognitive functions, and in turn, they have also emerged as a natural testbed for applying methods originally developed to probe information in neural populations. In this work, we utilize mean-field theoretic manifold analysis, a recent technique from computational neuroscience, to analyze the high dimensional geometry of language representations from large-scale contextual embedding models. We explore representations from different model families (BERT, RoBERTa, GPT, etc.) and find evidence for emergence of linguistic manifolds across layer depth (e.g., manifolds for part-of-speech and combinatorial categorial grammar tags). We further observe that different encoding schemes used to obtain the representations lead to drastic differences in whether these linguistic manifolds emerge in earlier or later layers of the network. In addition, we find that the emergence of linear separability in these manifolds is driven by a combined reduction of manifolds' radius, dimensionality and inter-manifold correlations.<sup>1</sup>

## 1. Introduction and Related Work

Many recent studies show notable similarities between representations extracted from task-optimized deep neural networks (DNNs) and neural populations in the brain in sensory systems (Yamins et al., 2014; Khaligh-Razavi & Kriegeskorte, 2014). Computational neuroscience community is increasingly relying on utilizing DNNs as a framework for studying neural correlates underlying complex cognitive functions (Cichy & Kaiser, 2019; Kriegeskorte, 2015). Addressing the question of "how a population of neural units transform representations across multilayered processing stages to implement a cognitive task" is a key challenge in both neuroscience and deep learning. Consequently, developing the techniques to provide insight into neural representation and computation have been an active area of research in both fields (Barrett et al., 2019).

Much prior work on characterizing how information is encoded in DNNs and the brain has focused on the geometric structure underlying the data. In neuroscience, representational similarity analysis (Kriegeskorte & Kievit, 2013) captures the similarity between the stimuli in the geometry of the neural data and deep network representations. Other geometric measures such as geodesics (Hénaff & Simoncelli, 2015), curvature (Hénaff et al., 2019; Fawzi et al., 2018), intrinsic dimension (Ansuini et al., 2019), and canonical correlation analysis (Raghu et al., 2017) have been used to empirically study the complexity of neural population and learned representations in DNNs.

In natural language processing (NLP), recent advances in contextualized word representations such as ELMo (Peters et al., 2018) and BERT (Devlin et al., 2018) have led to significant empirical improvements across many tasks. Concomitant with these advances is an emergent line of work, colorfully referred to as *BERTology*, exploring what aspects of language are being captured by these contextual representations. One popular approach for analysis is also through the lens of the geometry: Hewitt & Manning report evidence of a geometric representation of parse trees in embeddings from BERT, and Coenen et al. (2019) study the geometric representation of word senses via visualization techniques such as UMAP. Another popular approach for analyzing these representations is through *supervised probes*, i.e. clas-

<sup>\*</sup>Equal contribution <sup>1</sup>Intel AI Labs <sup>2</sup>Massachusetts Institute of Technology <sup>3</sup>Harvard University <sup>4</sup>Columbia University. Correspondence to: SueYeon Chung <sueyeon@mit.edu>.

*Proceedings of the 37<sup>th</sup> International Conference on Machine Learning*, Vienna, Austria, PMLR 108, 2020. Copyright 2020 by the author(s).

<sup>1</sup>Datasets, extracted features and code will be publicly available upon publication.

sifiers trained on top of fixed representations to predict certain linguistic properties (e.g., part-of-speech tags, syntactic heads). Supervised probes are conceptually simple and have greatly expanded our understanding of the kinds of linguistic knowledge encoded by these models. However, they are unable to capture the intrinsic geometry underlying the learned representation space, and it is not clear that high accuracy with respect to a probing task necessarily implies that the relevant linguistic structure is being encoded.

In this paper, we apply a recent manifold analysis technique based on replica theory (Chung et al., 2018) that links the geometry of object manifolds to the shattering capacity of a linear classifier as a measure of the amount of information stored about object categories per unit. This method has been used in sensory domains such as visual CNNs (Cohen et al., 2019), visual neuroscience (Chung et al., 2020) and deep speech recognition models (Stephenson et al., 2019) to characterize how object manifolds ‘untangle’ across layers. Here we apply this manifold analysis to study deep language representations, particularly Transformer-based models (Vaswani et al., 2017), for the first time, and show that NLP systems also ‘untangle’ linguistic ‘objects’ relevant for the task.

We present several key findings:

1. Word and linguistic category manifolds emerge across the deep layers of Transformer architectures, in the task-dependent, predictive regime (where the feature vectors are defined on masked tokens), similar to vision and speech deep networks.
2. In word contextualization regime (defined on unmasked tokens), word manifolds strongly decrease in the manifold capacity, becoming less separable across the hierarchy. Linguistic manifolds are affected by the underlying word manifolds, but are counteracted by the contextualization, resulting in linguistic manifolds with a better effective separation compared to word manifolds.
3. The emergence of part-of-speech manifolds is observed most strongly when the underlying words are ambiguous with multiple part-of-speech tags in BERT. Part-of-speech manifolds further seem to interpolate between word-like geometry and separable contextual geometry, depending on the number of words in each part-of-speech class.

In addition, we show the generality of linguistic untangling with word representation manifolds in widely-utilized NLP models. We also show that geometry of fine-tuning learning dynamics can be probed with the tasks congruent, incongruent to the training, to measure the similarity between the tasks. These results provide geometric evidence for emergence of language representation manifolds, from words to

part-of-speech to NER, in deep neural networks for natural language processing.

## 2. Mean-Field Theoretic Manifold Analysis

In this paper, we use the mean-field theoretic manifold analysis technique (Chung et al., 2018; Stephenson et al., 2019) (hereafter, MFTMA technique) to measure manifold capacity and other manifold geometric properties (radius, dimension, correlation) on a subsample of the test dataset.

Given  $P$  object manifolds (i.e. feature vectors with their categories) in  $N$  feature dimension, *Manifold capacity*,  $\alpha_C = P/N$ , refers to the critical number of object manifolds,  $P$ , that can be linearly separated given  $N$  features.  $\alpha_C$ , marks the value above which most manifold dichotomies are inseparable, below which most are separable. The manifold capacity thus measures the linearly separable information about object identity per feature. MFTMA returns four quantities below:

1. **Mean Field Theoretic (MFT) Manifold Capacity:** estimates the manifold capacity defined above, using the replica mean field formalism introduced in (Chung et al., 2018), and the code by (Stephenson et al., 2019)
2. **Manifold Dimension:** captures the dimensions of an object manifold, and estimates the average embedding dimension of the examples contributing to the decision hyperplane.
3. **Manifold Radius:** captures the size of the manifold relevant for linear separability. Small manifold radius implies that the set of examples that determine the decision boundary are tightly grouped.
4. **Center Correlations:** measures the average of pairwise correlations between manifold centroids.

Note that manifold capacity can also be computed empirically, and has been reported to be accurately predicted by MFT manifold capacity. We provide their consistency in our data in Supplementary Information (hereafter, SI). In this paper, we use MFT Manifold Capacity (hereafter, Manifold Capacity). The lower bound of the manifold capacity from data is given by (Cover, 1965), and reflects the case where there is no manifold structure. Manifold capacities in most random initialized DNNs closely follow lower bound capacity, and we find similar trends in language models (SI).

The key feature of MFTMA is that manifold capacity can be predicted by the geometric properties of the object manifolds, i.e., Manifold Dimension, Manifold Radius, and their center correlations. Small values for manifold radius, dimension and center correlation result in larger manifold capacity, rendering a more favorable geometry for classification.

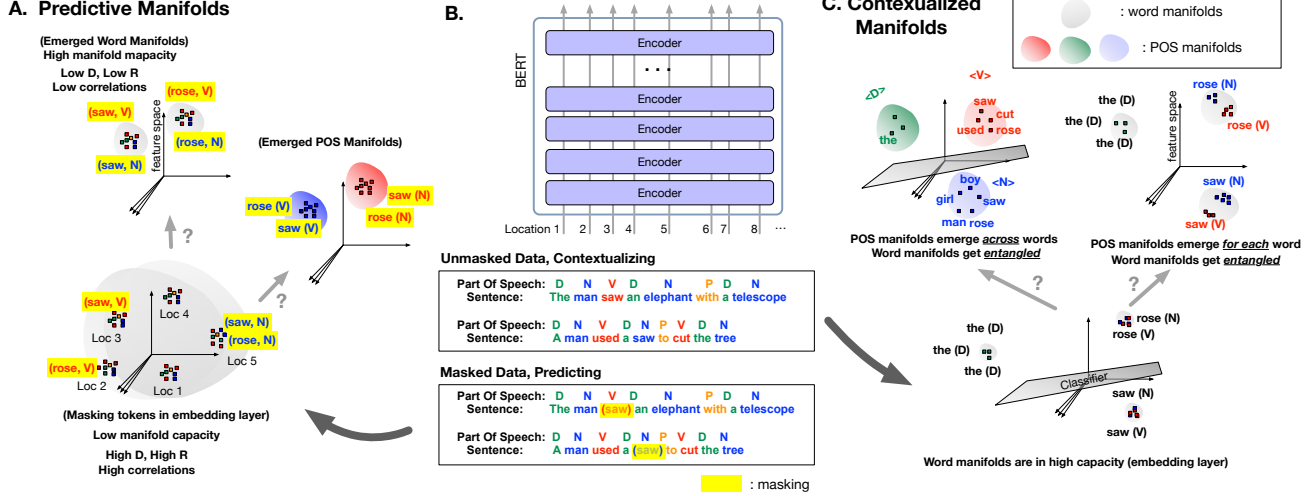


Figure 1. Emergence of word and linguistic manifolds across a Transformer hierarchy: (A) Predictive manifolds defined on masked tokens. (B) BERT hierarchy. (C) Contextualized manifolds defined on unmasked tokens.

### 3. Experimental Setup

We apply MFTMA to study the geometry of representations from a variety of contextualized word embedding models. We target Transformer-based models (Vaswani et al., 2017) which compose contextual representations at each layer with self-attention, as they have been shown to produce state-of-the-art results across a large number of NLP tasks. Transformer networks also provide an opportunity to analyze the evolution of representations across layer depth since they typically employ more hidden layers than other neural NLP models.

#### 3.1. Models

**BERT-based architectures:** BERT (Devlin et al., 2018) is a bidirectional Transformer pre-trained using a combination of masked language modeling objective and next sentence prediction on a large corpus. We also analyzed different architectures derived from BERT: RoBERTa (Liu et al., 2019b) modifies key hyperparameters in BERT including removing the next-sentence pre-training objective, and training with much larger mini-batches and learning rates; ALBERT (Lan et al., 2019) uses parameter-reduction techniques to lower memory consumption and increase the training speed of BERT; DistilBERT (Sanh et al., 2019) is a small, fast, cheap and light Transformer model trained by distilling BERT.

**GPT architecture:** OpenAI GPT (Radford et al., 2018) is a unidirectional left-to-right Transformer pre-trained using language modeling on a large corpus.

**Pretrained models:** We use the following model versions pretrained on English text: bert-base-cased, albert-base-v1, roberta-base, distilbert-base-uncased,

and openai-gpt. All the pre-trained models use a 12-layer transformer except distilbert-base-uncased that uses a 6-layer transformer and has hidden size of 768.

**Fine-tuned models:** In order to analyze how representations change when the model parameters are optimized towards a different task, we also test our approach on models fine-tuned on a downstream task (part-of-speech tagging) for different model training *updates steps*<sup>2</sup>

#### 3.2. Datasets and Manifold Definitions

As noted in section 2, MFTMA begins by assigning each representation to a particular linguistic category (i.e. manifold). We experiment with various word-level categories (derived from common NLP tasks/datasets) that target different language phenomena.

**Word:** A word manifold (word) contains several instances of the same word occurring in different contexts. We use the Penn Treebank (PTB) (Marcus et al., 1993) and select 80 word manifolds based on most frequent words in the corpus.

**Part-of-speech tags:** Part-of-speech (pos) tags consists of tags such as *proper nouns* (NNP), *determiners* (DT), etc., and are typically considered to target lower-level syntactic phenomena. We select the 33 most frequent tags from PTB.

**Semantic tags:** We use the semantic tagging (sem-tag) dataset from Abzianidze & Bos (2017), which annotates words with semantically informative tags. We take the 61 most-frequent semantic tags. Some examples of these tags include *comparative positive*, *concept*, *implication*, etc (we refer the reader to the original paper for the full tag definitions). This dataset has also been utilized to analyze

<sup>2</sup>as defined in [https://github.com/huggingface/transformers/blob/master/examples/run\\_ner.py](https://github.com/huggingface/transformers/blob/master/examples/run_ner.py)

contextual word representations in the context of supervised linear probes (Liu et al., 2019a).

**Named-entity recognition:** This task (ner) consists of locating and classifying named entity mentioned in text into pre-defined categories such as *person names*, *organizations*, *locations*, etc. It allows for finer-grained manifolds that other tasks since it involves additional segmentation using BIO (*begin*, *inside*, *outside*) tags. We use the tags from the Ontonotes dataset (Weischedel et al., 2011).

**Dependency depth:** All of the above datasets/tags (except words) have been studied by Liu et al. (2019a). Following Hewitt & Liang (2019), we study representations stratified by depth in a dependency tree (dep-depth). For each contextualized word representation, we use its depth in a dependency tree to assign it to a depth manifold. We select the 22 most frequent depths from PTB.

For each of the word-level tags defined above, we randomly sample 50 word instances per tag to perform the manifold analysis. We average the manifold metrics across five repetitions. For the rest of the paper, we use *linguistic manifolds* to refer to manifolds based on word, pos, sem-tag, ner and dep-depth. We further use *linguistic category manifolds* to refer to all linguistic manifolds except for dependency depth, since depth in a dependency tree is numeric.

### 3.3. Feature Extraction

BERT-based models are trained with a masked language modeling objective which randomly replaces words in a sentence with a special [MASK] token. We experiment with two encoding schemes for obtaining the contextualized representations in BERT-based models: *masked* and *unmasked*. In the *masked* case, we use the [MASK] token to obtain the contextualized representation, and assign the representation to the linguistic category of the predicted word (*predictive manifold* in Fig. 1). In the *unmasked* case, we obtain the contextualized word embedding by using the actual token as the input, correspondingly assign the representation to the linguistic category of the input (*contextualized manifold* in Fig. 1). In practice we observe that these two encoding schemes lead to differences in whether linguistic manifolds emerge in earlier or later layers of the network.<sup>3</sup>

If a word is tokenized into multiple tokens (subwords), its word representation is computed as the average of all its subwords' representations.

### 3.4. Methods

Our mean field theoretic manifold analysis closely follows prior work by Stephenson et al. (2019). We supplement the

<sup>3</sup> Voita et al. (2019) also analyze representations stratified by masked/unmasked representations, and report considerable differences the evolution of mutual information across layers.

manifold analysis with two additional techniques.

**Distribution of SVM Fields:** We analyze the distribution of fields (i.e. margins), defined as the signed perpendicular distance between the feature vector and the optimal linearly separating hyperplane using support vector machines (SVM). We train a slack-SVM with a linear kernel. Given  $P$  classes (e.g.  $P$  part-of-speech tags), we train SVM classifiers for one versus the rest classification task. The fields are measured only for the feature vectors with positive ground truth label (i.e. "one" of one vs. rest classification). For a given class, the fields from the true positives and false negatives are collected, and normalized by the field distance between the positive and negative class centroids. We collect these normalized fields from all  $P$  classes to finally obtain the distribution over fields. We also provide the similar analysis without the normalization (true perpendicular distances to the hyperplane) for reference in SI. The tail of the distribution on the positive side reflects a linear classification accuracy.

**PCA visualizations:** To qualitatively analyze the evolution of representations across layers, we visualize the representations with PCA, where each data point is color-coded according to its tag. When comparing representations across multiple layers, we perform PCA on data across all layers.

## 4. Results

### 4.1. Emergence of Separable Language Manifolds

**MFTMA analysis:** We first investigated the manifold capacity of Language Manifolds in the BERT model, which was trained to predict the word identity of the masked tokens in the output layer, using the datasets described in 3.2. The datasets have two forms: Masked, to observe the emergent properties of the task-dependent, predictive language manifolds, and Unmasked, to probe the information content in the contextualized word manifolds. The manifold capacity is presented as (1) the relative change compared to the embedding layer capacity (Fig 2, left column), and (2) normalized to the lower bound (right column, see Section 2) to enable comparison of the linguistic content embedded in the representations between different datasets.

Since the model is explicitly trained with masked modeling task on the word level, we observe that the word and other linguistic category manifold classes become more separable and increase in their capacity, over the course of the layers, on the masked data (Fig. 2B). Interestingly, other language classes based on POS, ner, sem-tag categories ("linguistic category manifolds") also emerges across the layers, and surprisingly, their relative increase across layers is comparable to the increase in word manifolds, perhaps reflecting the fact that the emergent linguistic category information is used to predict the masked words in the final layer.

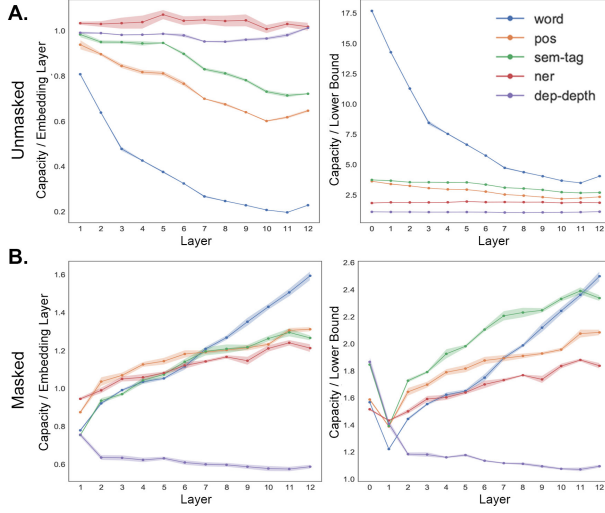


**Figure 2. Manifold capacity emerges across various linguistic tags in BERT** Manifolds defined by tags for words, POS, sem-tag, NER, dep-depth from (A) unmasked and (B) masked data (Note that empirical capacity matches MFT theory, SI). (Left column) MFT Manifold are normalized by the embedding layer manifold capacity for each tags ("Capacity/Embedding Layer"), to compare the effect of BERT layers. (Right column) MFT capacity is divided by their lower bound, for comparison of linear separability between different tasks. Error bars hereafter represent standard error on the mean of the calculated manifold metrics.

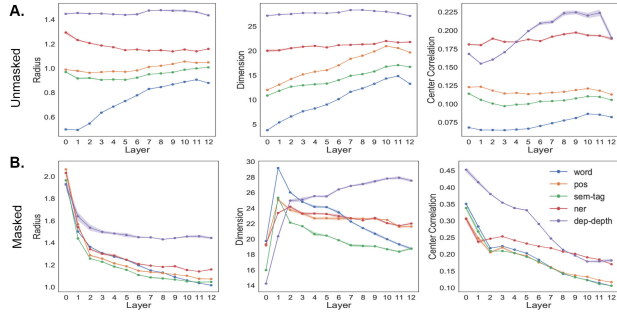


**Figure 3. Manifold Dimension, Radius, Correlations for various tasks in BERT** Manifolds defined by tags for words, POS, sem-tag, ner, dep-depth from (Top) unmasked and (Bottom) masked data.

On the unmasked data, since the word token is present in the input signal and is dominant, word capacity is much higher than the capacity in the masked data (Fig. 2A, right). As the input word embedding is already well separated, the word separability is at its highest in the embedding layer as expected. In subsequent layers, these highly separable word manifolds become contextualized and their capacity significantly decreases, as shown in Fig. 2A,B. For other language manifolds such as POS or ner, where the underlying representations are also based on word features (except

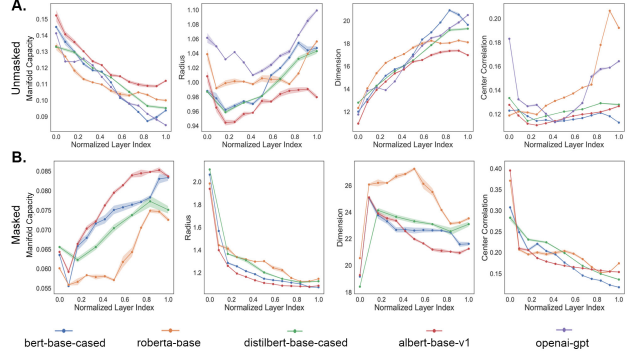


**Figure 4. Emergence of language manifolds across different transformer classes, shown by POS manifolds** (Top) (A) Manifold Capacity (B) Manifold Dimension (C) Manifold Radius (D) Center Correlations for all models overlaid on top of each other, for unmasked data (layers normalized) (Bottom) similar, for masked data (fewer models)

with language tags to define partitions based on linguistic categories), the capacity is similarly diminished, although not to the degree compared to the words manifold, due to the effect of the contextualization (Fig 3). Unlike the masked case, the linguistic manifolds have generally smaller capacity compared to words (Fig. 2A, right).

While the manifold capacity indicates an emergence of separable manifolds, the mean-field geometric metrics such as the manifold dimension, radius, and correlations tells us "how" the separability arises, i.e., theoretically-grounded geometric evidence of untangling. Across multiple tasks (POS, ner, ST, etc.), we find that for the masked data, the increased word and linguistic manifolds capacities are due to the reduction in the manifold radius, dimension, and center correlations (Fig. 3B), similar to prior work in vision and speech ((Stephenson et al., 2019)). For the unmasked case, the opposite trends are observed (Fig. 3A).

It's noteworthy that different linguistic categories show different relative trends. In manifold capacities (Fig. 2), in masked data, words, POS, sem-tag, ner show comparable amount of emergent capacity, while dep-depth shows a general reduction across layers. This might be due to the fact that dep-depth is based on depth of the tree, unlike other category-based tags, and classification-based metrics might not capture their functional and structural emergence. In unmasked data, a large decrease in the manifold capacity of POS (as compared to ner) potentially indicates that much POS tag information can be derived from words alone, which is consistent with the high accuracy of the most-frequent class baseline for POS tagging (Jurafsky & Martin, 2008). The trends in the capacity and geometry were similar across different Transformer architectures. The manifold capacities increase across the downstream layers, mediated by the reduction in the manifold dimension, radius, and

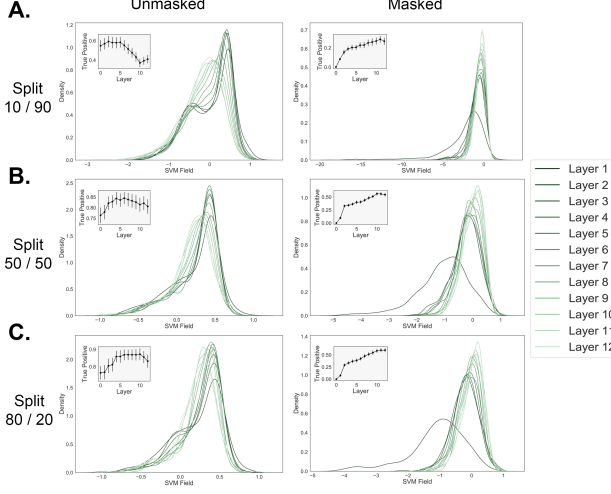


Figure 5. Emergence of linearly separable language manifolds

Fields distribution of POS Manifolds on (top left) unmasked and (top right) masked data, on center-normalized data with (Top) 80% Tr/ 20% Test Split, and (Bottom) 10% Tr/ 90% Test Split, on conditioned datasets (true positive + false negative). (Insets in each figure) Accuracy. (80/20 case is consistent with (Liu et al., 2019a), and 10/90 on unmasked data shows a different trend

center correlations in masked data, as shown in Fig. 4, as demonstrated by the POS manifolds (see SI for other linguistic tasks). In unmasked data, the capacity is higher overall compared to the capacity in masked data, and the manifold dimension, radius, and correlations are overall smaller, due to the existence of the strong signal in the input. The capacity of unmasked manifolds decrease, and this rate of decrease is steep in Word manifolds, but gradual in linguistic manifolds due to the contextualization effect (Fig. 4 for POS manifolds, and see SI for the rest of the linguistic manifolds across models).

**SVM fields statistics analysis:** We supplement the manifold capacity analysis by analyzing the statistics of the fields, i.e., the signed perpendicular distances between feature vectors and the SVM hyperplane, as described in Section 3.4. Figure 5 shows this for POS manifolds for different train-test splits, and across the BERT model layers. In the masked data (Fig. 5, left column), across all train/test splits, the peak of the fields distribution moves positively away from the origin from early to downstream layers, while the width gets smaller, meaning an increase in the signal to noise ratio, which is also reflected in the measured accuracy (Fig. 5, masked, Inset Figures). In the unmasked data, the peak of the fields distribution moves from the positive side to the origin (in the negative direction), across different train/test split regimes, showing the decreased separability, consistent with the trends observed in the manifold capacity. Interestingly, we find that the trend in linear separability, as measured by the accuracy across layer depth, is dependent on the size of

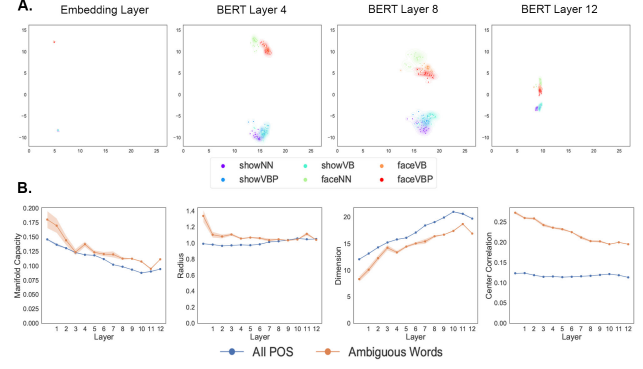


Figure 6. Emergence of POS manifolds in ambiguous words, unmasked data. (A) PCA visualization of Words with multiple possible POS tags. (B) Manifold capacity, radius, dimension, and center correlations of POS manifolds defined on ambiguous words, across the layers of BERT hierarchy.

the training set. With a train/test split of 10/90, the fraction of positive fields (i.e. accuracy) decreases across layers (Fig. 5, Top Left Inset). On the other hand, when we use the same train/test split of 80/20 used by Liu et al. (2019a), we recover their observation that the fraction of positive fields increases across the layers.

#### 4.2. Geometric Evidence for the Stronger Effect of Context in Ambiguous Words

Following our analysis of word and linguistic manifolds with metrics from both manifold theory and SVM fields, we searched for evidence of co-evolution of separable language manifolds of multiple types by visualizing their representations using PCA. We focus our analysis on two specific data: (1) words that occur across multiple part-of-speech tags, which we call "ambiguous words", and (2) open vs. closed part-of-speech tags (Lyons, 1977), corresponding to part-of-speech tags that have fixed class membership (closed tags) versus those that accept new members (open tags).

**Geometry of ambiguous words** Much of the part-of-speech information can be inferred by the choice of a word, regardless of the context, as some words always correspond to a specific part-of-speech (e.g., "the", "a", etc.). To test the additional information about part-of-speech tags gained by the neighboring context, we focus our analysis here on a specific set of words which occur across at least three different part-of-speech tags. This analysis is particularly useful because even for word manifolds, there is an effect of contextualization, observed by the steep decrease in the capacity across layers. Can we reduce the effect of underlying word manifolds by specifically choosing ambiguous words with multiple part-of-speech tags? The hypothesis here is that the amount of untangling of part-of-speech information might depend on how ambiguous underlying words are.

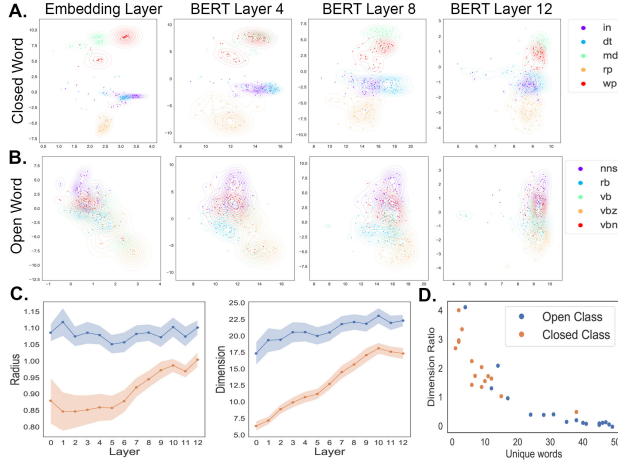


**Figure 7. Emergence of closed and open class POS Manifolds,** unmasked data: (A) Closed class POS manifolds. (B) Open class POS manifolds. (C) Manifold Radius, Dimension across layers. (D) Relative increase in POS manifold size, vs. number of words in POS class.

To test this, we first visualize word embeddings with multiple part-of-speech tags with PCA. We find that in the embedding layer, while the words are highly separated, different part-of-speech vectors are embedded very close to each other, and as the representations travel downstream, the part-of-speech sub-clusters within a same word (different colors) separate, while the overall manifold sizes get larger, clearly showing the competing effect of contextualization. This is a known challenge in the "untangling" deep networks, observed in vision; that is, the network needs to embed the whole data in high dimensional space, while separating and compressing the categorical data in low dimensional space, all using the same network parameters (Cohen et al., 2019; Recanatesi et al., 2019).

With the competing effect of contextualization on manifold geometry observed by PCA visualization, we then quantify these effects with our manifold analysis metric. One question is: while it's clear that the part-of-speech information is segregating conditioned on each word (Fig. 6, Top), are part-of-speech manifolds defined across many words also segregating, and do they segregate more, if the underlying words are ambiguous? Our results suggest that indeed BERT layers untangle POS manifolds from ambiguous words more than they untangle typical POS manifolds. In Fig. 6(B, left-middle), the typical decrease in the POS manifold capacity, typical increase in the radii and dimensions of the POS manifolds, compared to the embedding layer (blue) are alleviated in POS manifolds in ambiguous words (orange). In particular, radius and center correlations show a dramatic change in their qualitative trends (Fig. 6B): unlike in typical POS manifolds (blue), POS manifolds in ambiguous words get uncorrelated across layers, and their radii decrease, trends indicative an untangling in classifying

deep nets (Cohen et al., 2019; Stephenson et al., 2019).

We observe that this analysis can explain the ostensible contradiction between the decrease in manifold capacity across layer depth we measured and the increase in accuracy across layer depth that has generally been observed from supervised probes (Liu et al., 2019a). In particular, the visualizations indicate that there is an *overall* entangling of representations in later layers (when averaged across all words), leading to decrease in manifold capacity. However, there is an untangling of representations *within* each word, contributing to higher probe accuracy in later layers.

**Geometry of open vs. closed part-of-speech tags:** In addition to ambiguous words, we analyze part-of-speech classes with different number of words within each part-of-speech class, in unmasked data. We compare the geometry of closed class POS categories, corresponding to a small number of distinct words, and open class POS categories, with a large number of distinct words. Do closed-class POS manifolds show a similar geometrical transformation properties as word manifolds? Open-class manifolds, as embedded across many words, might be highly entangled in the input layer; do they show more emergent separability compared to closed-class manifolds?

Based on their PCA visualizations (Fig. 7A-B)), closed word POS classes are indeed already well separated in the embedding layer, and over the layers, these POS manifolds become more tangled, similar to the word manifolds trends seen previously (Fig. 7A). On the other hand, open POS classes are quite entangled in the beginning embedding layer, and their change in separability appears to be relatively small (Fig. 7B). Applying our manifold capacity method clearly shows that the measured manifold dimension and radii increases across layers in the closed class, but changes minimally for the open class (Fig. 7C). Finally, we quantify the effect of BERT hierarchy on the manifold's geometry as the Dimension Ratio =  $D_{output}/D_{input}$ , and observe that it's anti-correlated with the number of unique words in part-of-speech class. This result implies that the part of speech classes with a large number of words counteract the effect of expanding underlying word manifolds the most, signifying the structural evidence of contextualization on untangling of POS representations.

### 4.3. Geometry of Learning Dynamics and Task-transferability

In addition to evaluating the MFTMA metrics on the pre-trained networks, the analysis can also be done as the training progresses. Here, we trained a popular fine-tuning task, POS, on a pre-trained BERT, and trace the geometry of learned representations over the course of the training. Fig. 8A shows the evolution of representation geometry in different stages of learning epochs, measured by the capacity

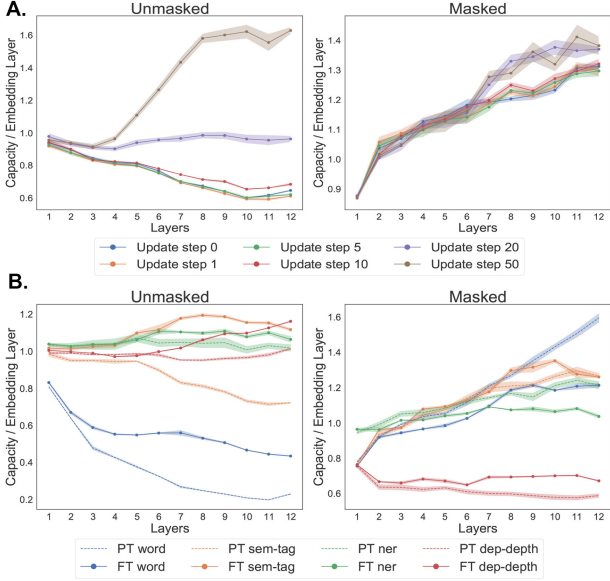


**Figure 8. Geometric evidence of fine tuning and task transfer representations** (Top) Emergence of POS manifolds on (left) unmasked, (right) masked data across update steps of POS fine-tuning on BERT. (Bottom) Linguistic manifolds on (left) unmasked, (right) masked data on (solid) final step of POS fine-tuning on BERT, compared with pretrained BERT (dashed).

of manifolds measured on the same tags as the training task (POS). Across training steps, POS manifolds in contextualizing regime (unmasked data) become more separable across layers, resulting in the regime where the manifold capacity increases across layers in the final step. Surprisingly, POS fine-tuning has little effect on masked data.

Furthermore, we characterize how these representations fine-tuned with POS task transfer to a different task, by measuring the manifold capacity with other linguistic tags, i.e., word, ner, sem-tag, and dep-depth. In unmasked data, the linguistic manifolds increase in their overall capacities with POS fine-tuning, showing the evidence of the task transfer. In masked data, most linguistic manifolds also improve in their capacity by a small amount, with an exception of word and NER manifolds, where an overall entanglement is observed between pretrained and fine-tuned models. Note that masked token is never seen during fine-tuning.

In addition, we supply the analysis on the manifold capacity vs. task performance (F1, precision, recall) across the fine-tuning updates in SI.

## 5. Discussion

In this paper, we studied the emergent geometric properties of word and linguistic object manifolds and their linear separability, as measured by the shattering manifold capac-

ity. Across different network models and datasets, we find that language manifolds emerge across the layers of the hierarchy. Particularly in the predictive manifolds defined on the masked data, the manifold capacity consistently increases, similar to the 'untangling' phenomena observed in visual and auditory sensory systems (Cohen et al., 2019; Chung et al., 2020; Stephenson et al., 2019). Contextualized manifolds defined on unmasked words also show implicit emergence of separable linguistic geometry, counteracting the strong entangling effect of word manifolds. Interestingly, the untangling effect of contextualization is stronger in words and linguistic tags that are ambiguous.

The emergence of increasing manifold capacity (accompanied by the emergent manifold geometry) on the masked data is reflective of the fact that the representations emerge across layers to become more "similar" to the last layer's output, consistent with the prior reports on the increasing mutual information between the intermediate and the last layers of contextual embedding models (Voita et al., 2019). The decrease of the word manifold capacity on unmasked data implies that information about the input word generally gets lost as representations get transformed downstream, similar to the reduced mutual information between input and intermediate layers (Voita et al., 2019). Furthermore, our metric goes beyond the constraints of the comparative measure, as the manifold capacity measures the amount of object information for any categories, allowing analysis of higher level linguistic categories such as POS.

Contextualization is a competition between gaining information from neighboring words, without losing information about the original word. Just as much as the original word representation is enhanced by the context, the same word representation is used to enhance the representation of other words. Measuring how distributed systems such as Transformers balance this multitude of information flows and implement linguistic information in a mixed representation is a theoretical challenge. Enabled by the recent manifold analysis technique, we report the quantifiable structural evidence of the evolution of language manifolds in connection to their linear separability in widely used language models.

Our methodology and results suggest many interesting future directions. We hope that our work will motivate: (1) the theory-driven geometric analysis of emergent representations underlying complex tasks such as prediction and contextualization; (2) the development of new theoretical frameworks that link the representation geometry and tasks with underlying causal structures; (3) the future study of language representations in the brain via the lens of geometry.

## References

Abzianidze, L. and Bos, J. Towards universal semantic tagging. *arXiv preprint arXiv:1709.10381*, 2017.

Ansuini, A., Laio, A., Macke, J. H., and Zoccolan, D. Intrinsic dimension of data representations in deep neural networks. In *Advances in Neural Information Processing Systems*, pp. 6109–6119, 2019.

Barrett, D. G., Morcos, A. S., and Macke, J. H. Analyzing biological and artificial neural networks: challenges with opportunities for synergy? *Current opinion in neurobiology*, 55:55–64, 2019.

Chung, S., Lee, D. D., and Sompolinsky, H. Classification and geometry of general perceptual manifolds. *Physical Review X*, 8(3):031003, 2018.

Chung, S., Dapello, J., Cohen, U., DiCarlo, J., and Sompolinsky, H. Separable manifold geometry in macaque ventral stream and dcnn. In *Computational and Systems Neuroscience (Cosyne)*, 2020.

Cichy, R. M. and Kaiser, D. Deep neural networks as scientific models. *Trends in cognitive sciences*, 2019.

Coenen, A., Reif, E., Yuan, A., Kim, B., Pearce, A., Viegas, F., and Wattenberg, M. Visualizing and Measuring the Geometry of BERT. In *Proceedings of NeurIPS*, 2019.

Cohen, U., Chung, S., Lee, D. D., and Sompolinsky, H. Separability and geometry of object manifolds in deep neural networks. *bioRxiv*, pp. 644658, 2019.

Cover, T. M. Geometrical and statistical properties of systems of linear inequalities with applications in pattern recognition. *IEEE transactions on electronic computers*, (3):326–334, 1965.

Devlin, J., Chang, M.-W., Lee, K., , and Toutanova, K. Bert: Pre-training of deep bidirectional transformers for language understanding. [abs/1810.04805](https://arxiv.org/abs/1810.04805), 2018. URL [http://arxiv.org/abs/1810.04805](https://arxiv.org/abs/1810.04805).

Fawzi, A., Moosavi-Dezfooli, S.-M., Frossard, P., and Soatto, S. Empirical study of the topology and geometry of deep networks. In *Proceedings of the IEEE Conference on Computer Vision and Pattern Recognition*, pp. 3762–3770, 2018.

Hénaff, O. J. and Simoncelli, E. P. Geodesics of learned representations. *arXiv preprint arXiv:1511.06394*, 2015.

Hénaff, O. J., Goris, R. L., and Simoncelli, E. P. Perceptual straightening of natural videos. *Nature neuroscience*, pp. 1, 2019.

Hewitt, J. and Liang, P. Designing and Interpreting Probes with Control Tasks. In *Proceedings of EMNLP*, 2019.

Hewitt, J. and Manning, C. D. A Structural Probe for Finding Syntax in Word Representations. pp. 10.

Jurafsky, D. and Martin, J. H. Speech and language processing: An introduction to speech recognition, computational linguistics and natural language processing. *Upper Saddle River, NJ: Prentice Hall*, 2008.

Khaligh-Razavi, S.-M. and Kriegeskorte, N. Deep supervised, but not unsupervised, models may explain it cortical representation. *PLoS computational biology*, 10(11), 2014.

Kriegeskorte, N. Deep neural networks: a new framework for modeling biological vision and brain information processing. *Annual review of vision science*, 1:417–446, 2015.

Kriegeskorte, N. and Kievit, R. A. Representational geometry: integrating cognition, computation, and the brain. *Trends in cognitive sciences*, 17(8):401–412, 2013.

Lan, Z., Chen, M., Goodman, S., Gimpel, K., Sharma, P., and Soricut, R. Albert: A lite bert for self-supervised learning of language representations, 2019.

Liu, N. F., Gardner, M., Belinkov, Y., Peters, M. E., and Smith, N. A. Linguistic knowledge and transferability of contextual representations. *CoRR*, abs/1903.08855, 2019a. URL [http://arxiv.org/abs/1903.08855](https://arxiv.org/abs/1903.08855).

Liu, Y., Ott, M., Goyal, N., Du, J., Joshi, M., Chen, D., Levy, O., Lewis, M., Zettlemoyer, L., and Stoyanov, V. Roberta: A robustly optimized bert pretraining approach, 2019b.

Lyons, J. Semantics (vol. 1 & vol. 2), 1977.

Marcus, M. P., Santorini, B., and Marcinkiewicz, M. A. Building a large annotated corpus of English: The Penn Treebank. *Computational Linguistics*, 19(2):313–330, 1993. URL <https://www.aclweb.org/anthology/J93-2004>.

Peters, M., Neumann, M., Iyyer, M., Gardner, M., Clark, C., Lee, K., and Zettlemoyer, L. Deep contextualized word representations. In *Proceedings of the 2018 Conference of the North American Chapter of the Association for Computational Linguistics: Human Language Technologies, Volume 1 (Long Papers)*, pp. 2227–2237, New Orleans, Louisiana, June 2018. Association for Computational Linguistics. doi: 10.18653/v1/N18-1202. URL <https://www.aclweb.org/anthology/N18-1202>.

Radford, A., Narasimhan, K., Salimans, T., and Sutskever, I. Improving language understanding by generative pre-training. URL <https://radfordai.github.io/language-models/>.

<https://s3-us-west-2.amazonaws.com/openai-assets/researchcovers/languageunsupervised/languageunderstandingpaper.pdf>, 2018.

Raghuram, M., Gilmer, J., Yosinski, J., and Sohl-Dickstein, J. Svcca: Singular vector canonical correlation analysis for deep learning dynamics and interpretability. In *Advances in Neural Information Processing Systems*, pp. 6076–6085, 2017.

Recanatesi, S., Farrell, M., Advani, M., Moore, T., Lajoie, G., and Shea-Brown, E. Dimensionality compression and expansion in deep neural networks. 2019.

Sanh, V., Debut, L., Chaumond, J., and Wolf, T. Distilbert, a distilled version of bert: smaller, faster, cheaper and lighter. 2019.

Stephenson, C., Feather, J., Padhy, S., Elibol, O., Tang, H., McDermott, J., and Chung, S. Untangling in invariant speech recognition. In *Advances in Neural Information Processing Systems*, pp. 14368–14378, 2019.

Vaswani, A., Shazeer, N., Parmar, N., Uszkoreit, J., Jones, L., Gomez, A. N., Kaiser, L., and Polosukhin, I. Attention Is All You Need. In *Proceedings of NeurIPS*, 2017.

Voita, E., Sennrich, R., and Titov, I. The Bottom-up Evolution of Representations in the Transformer: A Study with Machine Translation and Language Modeling Objectives. In *Proceedings of EMNLP*, 2019.

Weischedel, R., Hovy, E., Marcus, M., Palmer, M., Belvin, R., Pradhan, S., Ramshaw, L., and Xue, N. Ontonotes: A large training corpus for enhanced processing. *Handbook of Natural Language Processing and Machine Translation*. Springer, pp. 59, 2011.

Yamins, D. L., Hong, H., Cadieu, C. F., Solomon, E. A., Seibert, D., and DiCarlo, J. J. Performance-optimized hierarchical models predict neural responses in higher visual cortex. *Proceedings of the National Academy of Sciences*, 111(23):8619–8624, 2014.

000  
001  
002  
003  
004  
005  
006  
007  
008  
009  
010  
011  
012  
013  
014  
015  
016  
017  
018  
019  
020  
021  
022  
023  
024  
025  
026  
027  
028  
029  
030  
031  
032  
033  
034  
035  
036  
037  
038  
039  
040  
041  
042  
043  
044  
045  
046  
047  
048  
049  
050  
051  
052  
053  
054

## 1. Appendix

### 1.1. Empirical manifold capacity and theoretical manifold capacity

#### 1.1.1. EMPIRICAL MANIFOLD CAPACITY

In this section, we provide detailed description about how to find empirical manifold capacity. Given  $P$  object manifolds,  $N_c$ , the critical number of feature dimensions, is defined as the necessary number of feature dimensions so that  $P$  object manifolds, with randomly assigned  $+/ -$  labels for each manifold, can be linearly separated half the time on average (see (?)). The empirical manifold capacity is defined as  $P/N_c$ , which is the ratio between number of object manifold and the critical number of feature dimensions. To find  $N_c$ , a bisection search is performed until either the linearly separated fraction is within an error tolerance range  $\epsilon = 0.05$  or the number of iteration exceeds 100. If the number of feature dimensions  $N$  is larger than  $N_c$ , then the fraction of linearly separable dichotomies is close to 1, and the data is in the linearly separable regime. Conversely, if the number of feature dimensions  $N$  is smaller than  $N_c$ , then the fraction of linearly separable dichotomies is close to 0, and the data is in the linearly inseparable regime.

In our experiments, we first randomly sample 20 instances for each manifold to perform the analysis. Then, for each candidate feature dimension in the bisection search, we sample 51 randomly assigned dichotomies to compute the linearly separable fraction. We use features extracted from pre-trained bert-base-cased model. Note that we exclude the embedding layers in this analysis due to the overlapping data point between manifolds as reported in Section 1.3.

#### 1.1.2. THEORETICAL MANIFOLD CAPACITY

Theoretical capacity used here is Mean-Field Theoretical Manifold Capacity described in Section 2 of the main text. We use  $\kappa = 10^{-8}$  and  $n_t = 300$ , in which  $\kappa$  is the margin size and  $n_t$  is the number of Gaussian vectors to sample per manifold (see (?)). We also use the same randomly chosen 20 instances from the simulation capacity analysis for each manifold.

Figure 1 shows a close match between simulation capacity and the MFT manifold capacity observed in various linguistic tasks, measured across the hierarchy of bert-base-cased model.

## 1.2. Model architecture details

### 1.2.1. PRE-TRAINED MODELS DETAILS

We present briefly the pre-trained models that we used for the experiments.

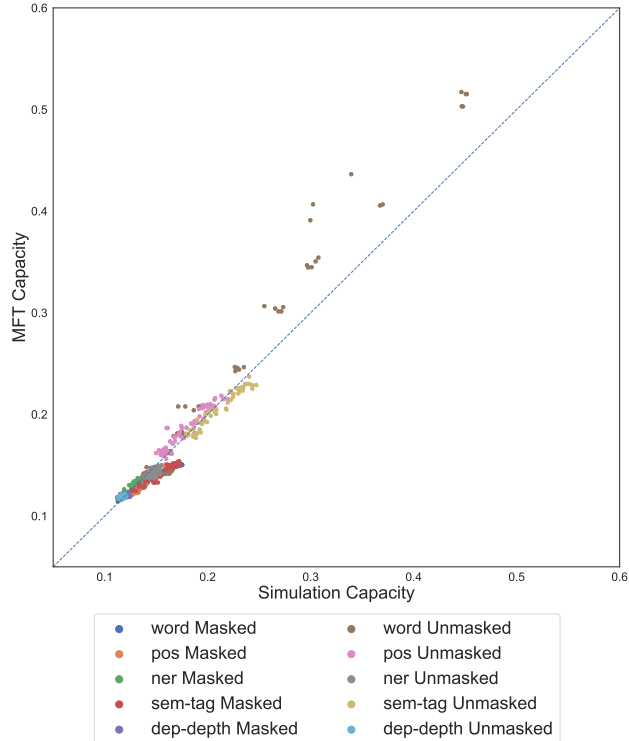


Figure 1. Simulation capacity vs. MFT capacity in bert-base-cased model.

- **BERT** bert-base-cased. 12-layer, 768-hidden, 12-heads, 110M parameters.
- **RoBERTa** roberta-base. 12-layer, 768-hidden, 12-heads, 125M parameters.
- **ALBERT** albert-base-v1. 12 repeating layers, 128 embedding, 768-hidden, 12-heads, 11M parameters.
- **DistilBERT** distilbert-uncased. 6-layer, 768-hidden, 12-heads, 66M parameters. The model distilled from the BERT model bert-base-uncased checkpoint.
- **OpenAI-GPT** openai-gpt. 12-layer, 768-hidden, 12-heads, 110M parameters.

For each pre-trained model, input text is tokenized using its default tokenizer and features are extracted at token level.

### 1.2.2. FINE-TUNED MODEL DETAILS

We fine-tuned BERT bert-base-cased model on POS downstream task with the following hyper-parameters:

- Epsilon for Adam optimizer: 1e-8.

---

055     • Initial learning rate for Adam: 5e-5.  
 056     • Max gradient norm: 1.  
 057     • Maximum total input sequence length after tokeniza-  
 058       tion: 128. Longer sequences are truncated and shorter  
 059        sequences are padded.

060     **1.3. Datasets and Manifolds Details**

061     In this section, we provide some information about the labels  
 062       defining the manifolds for each task with some additional  
 063       details (e.g., overlapping).

064       **1.3.1. WORD**

065     Labels are the following: the, of, to, in, and,  
 066       for, that, is, it, said, on, at, by,  
 067       as, from, with, million, was, be, are,  
 068       its, he, but, has, an, will, have, new,  
 069       or, company, they, this, year, which,  
 070       would, about, says, market, more, were,  
 071       his, billion, had, their, up, one,  
 072       than, some, who, been, stock, also,  
 073       other, share, not, we, when, last, if,  
 074       years, shares, all, president, first,  
 075       two, sales, after, inc., because,  
 076       could, out, trading, there, only,  
 077       business, do, such, can, most, into.

078     Note that, by definition, there is no overlapping between the  
 079       manifolds.

080       **1.3.2. PART-OF-SPEECH**

081     Labels are the following: NN, IN, NNP, DT, JJ,  
 082       NNS, CD, RB, VBD, VB, CC, TO, VBZ, VBN,  
 083       PRP, VBG, VBP, MD, POS, PRP\$, WDT, JJR,  
 084       NNPS, RP, WP, WRB, JJS, RBR, EX, RBS,  
 085       PDT, FW, WP\$.

086     Labels are described in [https://www.ling.upenn.edu/courses/Fall\\_2003/ling001/penn\\_treebank\\_pos.html](https://www.ling.upenn.edu/courses/Fall_2003/ling001/penn_treebank_pos.html).

087     There is 0.032% of overlapping pairs of words in the  
 088       embedding layer due to the occurrence of a same word at  
 089       the same position in multiple sentences with a different  
 090       POS label. However, as expected, there is no overlapping  
 091       for higher layers.

092     For the POS open-word class and closed-word class  
 093       analysis, we used the following assignment of POS tags:

094       • Open-word class: JJ, JJR, JJS, RB, RBR,  
 095        RBS, NN, NNS, NNP, NNPS, VB, VBD,  
 096        VBG, VBN, VBP, VBZ, FW

097       • Closed-word class: IN, DT, CD, CC, TO,  
 098        PRP, MD, POS, PRP\$, WDT, RP, WP,  
 099        WRB, EX, PDT, FW, WP\$

100     For the ambiguous words analysis, we used the fol-  
 101       lowing words with associated POS tags: back (RP,  
 102       RB, JJ, NN), cut (VBN, VBD, NN, VB),  
 103       set (VBD, VB, NN, VBN), close (NN, RB,  
 104       JJ, VB), lower (RBR, VB, JJR), closed  
 105       (VBD, VBN, JJ), estimated (JJ, VBD,  
 106       VBN), call (NN, VB, VBP), come (VB,  
 107       VBN, VBP), earlier (JJR, RBR, RB), pay  
 108       (VB, VBP, NN), up (RP, RB, IN), over  
 109       (IN, RB, RP), proposed (JJ, VBN, VBD),  
 110       face (VBP, VB, NN), continued (JJ, VBD,  
 111       VBN), down (IN, RB, RP), show (VB, VBP,  
 112       NN), off (RP, RB, IN), better (JJR,  
 113       RBR, RB), longer (RBR, RB, JJR), half  
 114       (NN, PDT, DT), expected (VBN, JJ, VBD),  
 115       buy (VB, NN, VBP), look (VB, NN, VBP)

116       **1.3.3. SEMANTIC TAGS**

117     Labels are the following: CON, REL, IST, DEF,  
 118       LOC, PST, ORG, PER, DIS, SUB, EXS, NOW,  
 119       PRO, HAS, AND, EXG, EXV, QUA, GPE, EXT,  
 120       ENT, TIM, COO, APP, EPS, YOC, FUT, DOM,  
 121       NOT, MOR, MOY, ENG, INT, TOP, ALT, ENS,  
 122       ETV, POS, PRX, BUT, EPT, UOM, DST, QUE,  
 123       NEC, EPG, IMP, ART, HAP, ETG, ROL, DOW,  
 124       SCO, REF, COM, DEC, EXC, NAT, RLI, LES,  
 125       EFS.

126     Labels are described by ?.

127     Note that there is no overlapping between the manifolds.

128       **1.3.4. NAMED-ENTITY RECOGNITION**

129     The NER dataset includes 18 labels described by ?, consist-  
 130       ing of 11 types (GPE, LOCATION, WORK\_OF\_ART,  
 131       EVENT, LAW, PRODUCT, LANGUAGE, PERSON,  
 132       ORG, NORG, FAC) and 7 values (DATE, PERCENT,  
 133       CARDINAL, TIME, QUANTITY, ORDINAL,  
 134       MONEY). With BIO tagging scheme, each label can  
 135       occur either with B- (*beginning*) prefix or with I- (*inside*)  
 136       prefix; there is an additional O (*outside*) label for words that  
 137       are not named-entities.

138     There is 0.014% of overlapping pairs of words in the em-  
 139       bedding layer due to the occurrence of a same word at the  
 140       same position in multiple sentences with a different NER  
 141       label. However, as expected, there is no overlapping for  
 142       higher layers.

## 110 1.3.5. DEPENDENCY DEPTH

111 We select dependency depths from 0 to 21. From depth 18  
112 to 21, we have respectively 12, 12, 5, 4 samples occurring  
113 in the corpus (instead of 50 for other depths).

114 Note that there is no overlapping between the manifolds.

## 115 1.4. Additional Experiments

116 1.4.1. RANDOM BASELINE CONTROL FOR MANIFOLD  
117 CAPACITY118 We compare in Figure 2 the manifold capacity to three  
119 different manifold capacity baselines:120 • **Lower bound.** The lower bound capacity  $LB$  is defined as the classification capacity of unstructured manifolds and only depends on the number of samples in each manifold.

121 
$$LB = \frac{1}{\frac{1}{n} \sum_{i=1}^n \frac{l_i}{2}} \quad (1)$$

122 where  $LB$  is lower bound capacity,  $n$  is the number of  
123 manifolds,  $l_i$  is the number of samples in manifold  $i$   
124 (see (?)).125 • **Randomly initialized (untrained) model.** All model  
126 weights are set to a random number. Note that this ran-  
127 dom initialization has also an impact on the embedding  
128 layer.  
129  
• **Shuffled label manifolds.** The manifolds are shuffled  
130 without repetition and the number of samples for each  
131 manifold are preserved.132 For both masked and unmasked data from  
133 bert-base-cased model, the capacity of shuffled label  
134 manifolds matches closely with the lower bound  
135 capacity, suggesting that randomly assigned manifold in  
136 different layers and linguistic tasks follow closely with  
137 the lower bound capacity.138 Concerning the untrained model with random weights, in  
139 unmasked data, the capacities in the embedding layer are  
140 higher than lower bound and lower than the capacities in the  
141 pre-trained model. This reflects the fact that word vectors  
142 are already somewhat separated in the embedding layer, and  
143 the random weights don't improve or decrease the capacity.  
144 For the masked data with untrained model, the manifold  
145 capacity decreases across layers. The trends observed here  
146 are similar to prior work by ?. Note that as observed by  
147 ?, structured manifolds could emerge even in untrained  
148 models.149 1.4.2. ANALYSIS OF RAW SVM FIELDS DISTRIBUTION  
150 OF POS MANIFOLD151 We report in Figure 3 the raw SVM fields distribution of  
152 POS manifold with bert-base-cased model. The raw  
153 SVM fields distribution, despite of having a different dis-  
154 tribution shape, shows similar trend across layers with the  
155 normalized SVM fields distribution described in the main  
156 text for both masked and unmasked dataset. The accuracy  
157 for raw SVM field distribution matches exactly the accuracy  
158 for normalized SVM fields distribution because normaliza-  
159 tion doesn't change sign of the fields. For unmasked data,  
160 the peak of the field distribution and the right tail moves  
161 slightly to the negative direction in all different train/test  
162 splits. For masked data, although the peak shifts to the neg-  
163 ative direction, the right tail of the distribution extends to  
164 the positive direction in all different train/test splits, repre-  
165 senting an increase in accuracy across layers.166 1.4.3. GEOMETRIC PROPERTIES EVOLUTION THROUGH  
167 SEQUENTIAL LAYERS ACROSS LINGUISTIC  
168 TASKS AND MODELS (ADDITIONAL FIGURES)169 We report geometric properties (manifold capacity, radius,  
170 dimension and center correlation) for word, semantic tags,  
171 NER and dependency depth manifolds for the different mod-  
172 els.173 **Word** For word manifolds, as reported in Figure 4, simi-  
174 larly to POS manifold, the capacity increases for unmasked  
175 data and decreases for masked data in all the different mod-  
176 els. In both masked and unmasked cases, the trend is clear  
177 and steep. In the masked case, the inputs are masked and  
178 feature vectors values only depend on the positional em-  
179 bedding and are not related to the word strings; since the  
180 model is trained to predict the masked word token, the word  
181 manifolds emerge across layers. In the unmasked case, the  
182 inputs are context-free embedding word vectors and are  
183 well separated; since the model tries to contextualize the  
184 word using its neighbor words, the word manifolds get en-  
185 tangled and lead to a decrease in word manifold capacity.  
186 The radius, dimension and center correlation measures also  
187 reflect the observed trend in the capacity. In the unmasked  
188 data, the radius, the dimension and center correlation of  
189 word manifolds increase across layers, representing mani-  
190 fold entangling. In the masked data, the dimension, radius  
191 and center correlation decrease across layers, suggesting  
192 manifold untangling.193 **Semantic Tags** For semantic tag manifolds, as reported  
194 in Figure 5, similarly to word manifolds and POS manifolds,  
195 the capacity decreases in the unmasked dataset and increases  
196 in the masked dataset. Similarly to POS tags, semantic tags  
197 also have high correlation with context-free word; as re-  
198 ported by ?, the per-word most frequent class baseline for

165  
166  
167  
168  
169  
170  
171  
172  
173  
174  
175  
176  
177  
178  
179  
180  
181  
182  
183  
184  
185  
186  
187  
188  
189  
190  
191  
192  
193  
194  
195  
196  
197  
198  
199  
200  
201  
202  
203  
204  
205  
206  
207  
208  
209  
210  
211  
212  
213  
214  
215  
216  
217  
218  
219

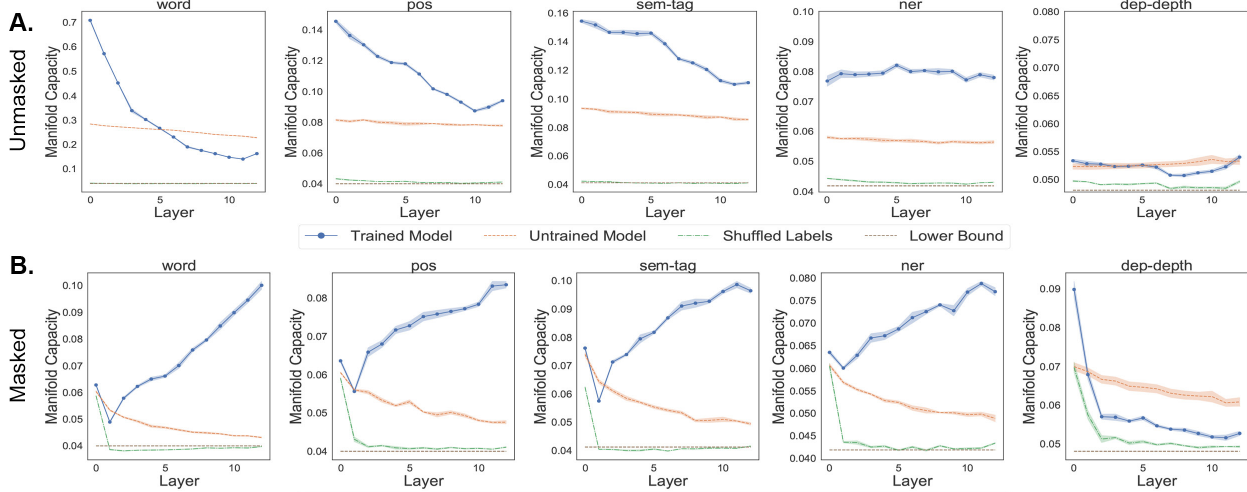


Figure 2. Randomly controls for manifold capacity in bert-base-cased model.

semantic tags has an accuracy of 77.39%. Therefore, in the masked case, since the model is trained to predict the word tokens which share information with the semantic tags, the manifold capacity increases. In the unmasked case, the inputs are word embedding vectors, which carry information about semantic tags, and the model tries to contextualize the inputs by their neighboring words. Contextualization can both entangle semantic tags manifold by decreasing the correlation between word tokens and their semantic tags and untangle semantic tags manifold by gaining information from neighbor words. These two competing effects lead to an overall decrease in manifold capacity, but this decrease has a much less magnitude than the decrease in word manifold capacity ( $-0.6$  vs.  $-0.06$ ). Manifold radius, dimension and center correlation also have similar trend as POS and word manifolds.

**Named-entity Recognition** For NER manifolds, as reported in Figure 6, the different models express similar trend for both masked and unmasked data. For the unmasked data, the manifold capacity remains mostly unchanged across layers. This trend suggests a balance between losing information from correlation between words and NER label, and gaining information from contextualization by neighbor words. The geometric properties also show a competing effect between decreasing radius and increasing dimension and center correlation. For the masked data, the manifold capacity increases across layers (similar trend as word, POS and sem-tag). This trend is expected because the input tokens are masked and the model objective is to predict the masked word, which can carry some information about NER. Geometric properties show decreasing radius and center correlation, suggesting manifold untangling.

**Dependency Depth** For dependency depth manifolds, as reported in Figure 7, similar trend is observed for the different models in both masked and unmasked dataset. For unmasked data, the manifold capacity remains mostly unchanged. Manifold radius and dimension do not change significantly, while center correlation peaks at the intermediate layers. Since dependency depths are numerical values, higher center correlation may suggest a structured geometry relationship between different dependency depth clusters. ? also reports similar results about syntactic parse tree peaks at the intermediate layers. For masked data, manifold capacity, radius and center correlation decreases across layers, while dimension increases. Generally, the manifold capacity and geometry measures for dependency depth manifolds are quite different from other manifolds. While other manifolds are *categorical* values, dependency depths are *numerical* values. A large capacity implies that category manifolds are well-separated for a classification task; however, since dependency depth manifolds have a numerical and transitive property, its geometry may not be optimized for classification capacity. Instead, dependency depth task may be explained better by a task that reflects such numerical and transitive properties such as a regression task, and the relation between the representation geometry and the regression performance will be explored as future work.

#### 1.4.4. CORRELATION OF MANIFOLD CAPACITY AND TASK PERFORMANCE IN POS FINE-TUNED MODEL

When fine-tuning pre-trained bert-base-cased model for POS task, a strong correlation is observed between the POS manifold capacity and F1 score across update steps for unmasked data, as reported in Table 1 and Table 2. Specifi-

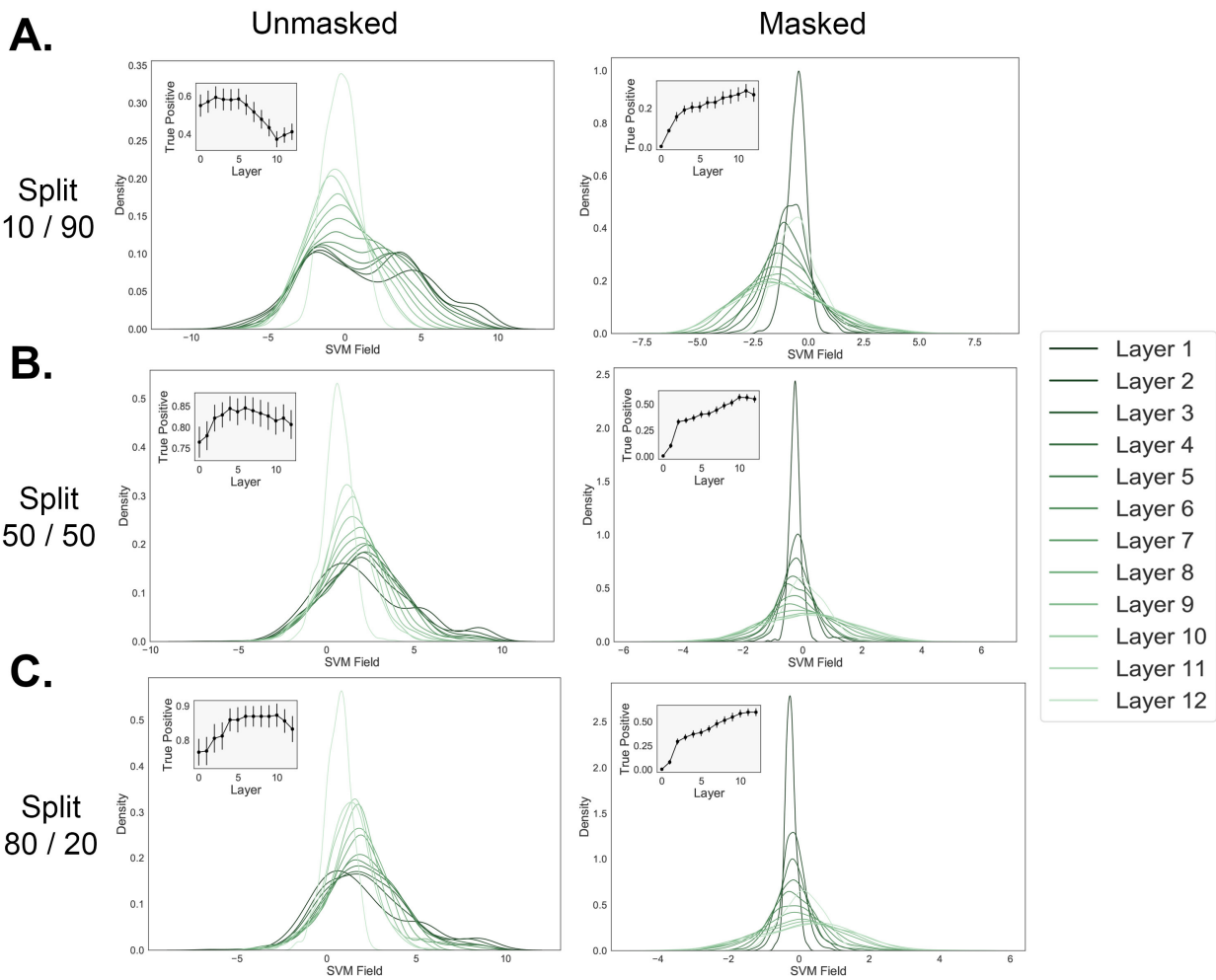


Figure 3. Raw SVM fields of POS manifold with bert-base-cased model.

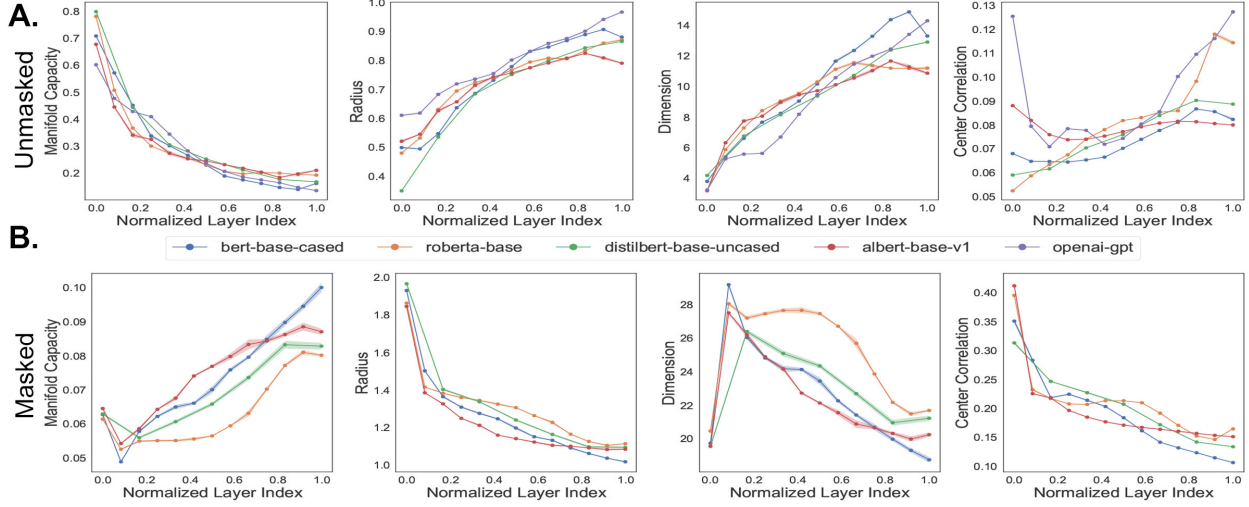


Figure 4. Geometric properties of word manifold in different models.

update step	raw capacity	F1
1	0.0903	0.04
5	0.0915	0.11
10	0.0998	0.34
20	0.1362	0.55
50	0.2361	0.87
Pearson correlation		0.9334

Table 1. Correlation of raw manifold capacity and F1 in POS fine-tuned model, unmasked data.

update step	norm. capacity	F1
1	0.6111	0.04
5	0.6209	0.11
10	0.6839	0.34
20	0.9623	0.55
50	1.6274	0.87
Pearson correlation		0.9417

Table 2. Correlation of manifold capacity (normalized by embedding layer) and F1 in POS fine-tuned model, unmasked data.

318 cally, Pearson correlation for raw capacity and F1 score and  
 319 for normalized capacity and F1 score are 0.9334 and 0.9417  
 320 respectively. This result suggests that manifold capacity can  
 321 capture task performance (F1 score) in POS task. Note that  
 322 asked data is not shown because masked token is never seen  
 323 during fine-tuning.

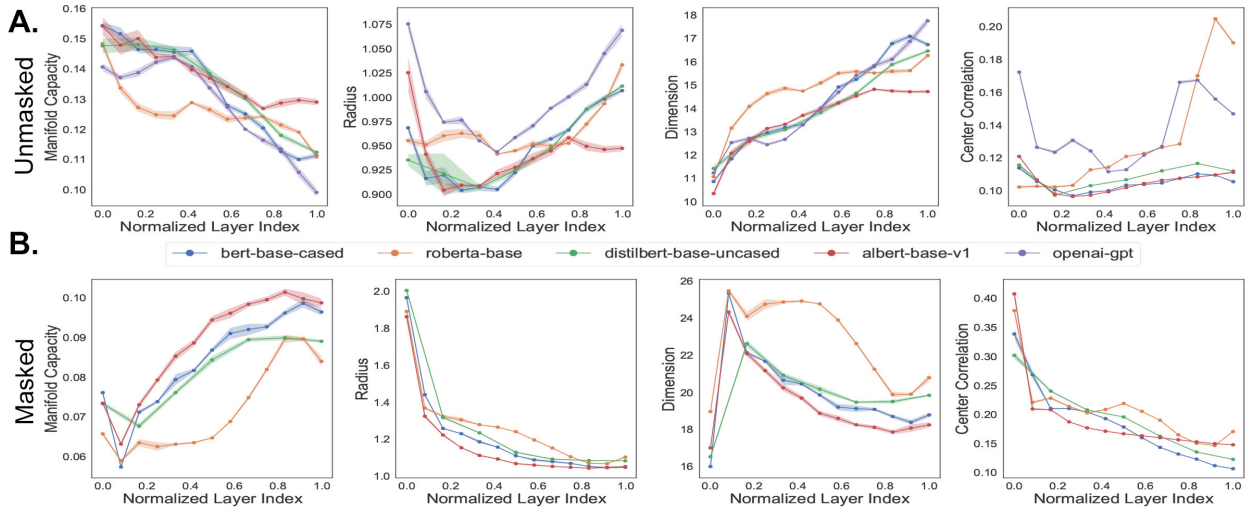


Figure 5. Geometric properties of semantic tags manifold in different models.

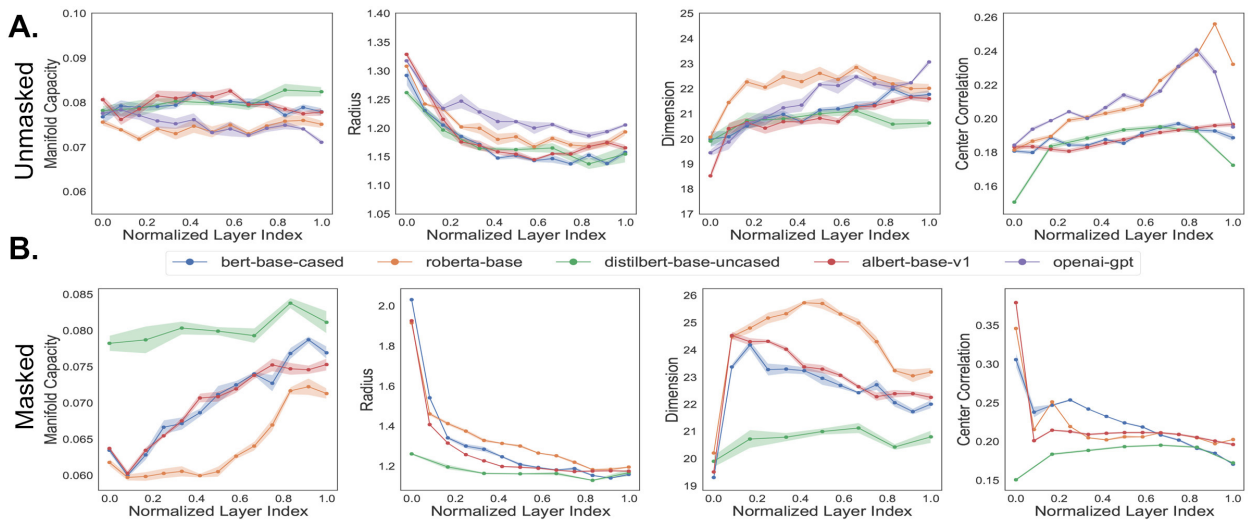


Figure 6. Geometric properties of NER manifold in different models.

385  
386  
387  
388  
389  
390  
391  
392  
393  
394  
395  
396  
397  
398  
399  
400  
401

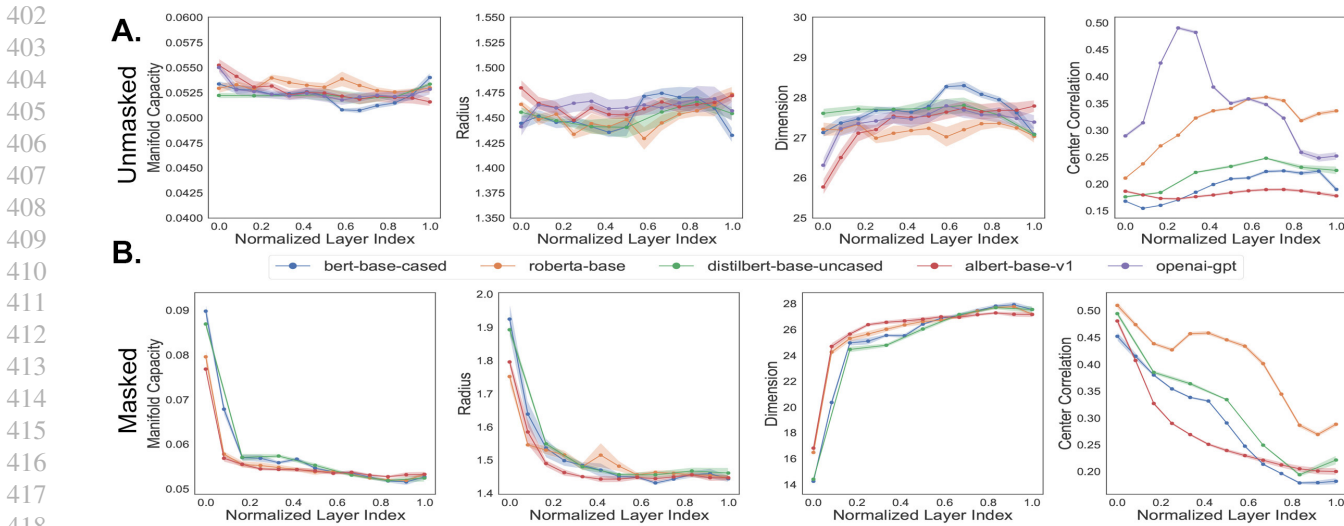


Figure 7. Geometric properties of dependency depth manifold in different models.